scientific reports

OPEN

Formation of surface states on Pb(111) by Au adsorption

Wei-Chuan Chen[1,5], Chin-Hsuan Chen[1,5], Angus Huang[1], Kaweng Lei[1], David Mikolas[1], Ming-kwan Dai[1], Je-Ming Kuo[1,2], Dai-Shien Lin[1], Cheng-Maw Cheng[2], H.-T. Jeng[1,3,4✉] & S.-J. Tang[1,2,3✉]

Using low-energy electron diffraction and angle-resolved photoemission spectroscopy, we investigated the lattice and electronic structures of the Pb(111) surface upon the adsorption of Au atoms at the low temperature $T = 40$ K. Unlike earlier results showing the formation of PbAu-alloy layers at room temperature, we found that Au atoms form a ultra-thin superstructure, Au/Pb(111)-3×3, on top of the Pb(111) surface. Moreover, three surface-state bands, S_1, S_2, and S_3, are induced within and immediately adjacent to the Pb bulk projected band gap centered at the surface zone boundary $\overline{M}_{Pb(111)}$ at the energies of – 0.02, – 1.05, and – 2.56 eV, respectively. First-principles calculation based on Au/Pb(111)-3×3 confirms the measured surface-state bands among which the most interesting are the S_1 and S_3 surface states. They are derived from surface resonances in Pb(111). Moreover, S_1, which disperses across Fermi level, exhibits a large anisotropic Rashba splitting with α of 1.0 and 3.54 eVÅ in the two symmetry directions centered at $\overline{M}_{Pb(111)}$. The corresponding Rashba splitting of S_1 band in Cu/Pb(111)-3×3 and Ag/Pb(111)-3×3 were calculated for comparison.

Bulk Pb is well known to be a conventional s-wave superconductor with a fairly high transition temperature of superconductivity T_C of 7.23 K[1]. Based on the measured cyclotron effective mass, the renormalization factor λ (the so-called electron–phonon coupling strength) was extracted to have a high value up to 1.5[2]. It was not until 1980s that attention started to focus on the atomically uniform Pb thin films, for which measured T_C values exhibit bilayer-oscillatory dependence on thickness[3]. The same oscillatory behavior was also observed for electron–phonon coupling strength λ by investigating the temperature dependence of hole lifetime of quantum well states (QWS)[4]. The bilayer oscillations of T_c and λ were attributed to the variation of density of states (DOS) at the Fermi level, exclusively determined by the energy positions of QWS. However, the superconductivity as well as the electron–phonon interaction at the surfaces of bulk Pb and Pb thin films have been long overlooked because of the lack of localized surface states (SS)[5,6]. On the other hand, the Pb atom itself has strong spin–orbit coupling (SOC)[7]; therefore a large Rashba effect at the surfaces of Pb bulk or thin films was expected but has never been observed for the same reason. Nevertheless, a weak Rashba effect was observed from QWS of flat Pb thin films[8]. This can be understood in light of the fact that the QWS wavefunction distributes between two interfaces (vacuum/film and film/substrate) and the out-of-plane potential gradients derived from both oppose. The Rashba effect is thus smeared out.

Therefore, to explore the superconductivity and Rashba effect at the Pb(111) surface, pronounced and localized SS's are indispensable. The experimental observation of SS in metal surfaces was more difficult than in semiconductor surfaces[9]. The main reason is that metal crystals have partial bulk band gaps rather than the complete bulk band gaps that exist in semiconductors. The first experimental observation and proof of SS in a metal surface was made from the transition metal, W(100), by E. W. Plummer and J. W. Gadzuk[10] using field emission measurement. Wurde et al.[5] pointed out that the well separated s, p, and d bands in bulk Pb makes the formation of SS due to hybridization less possible than in transition metals. In addition, the higher coordination of Pb atoms at nearest and next-nearest neighbors on the (111) surface compared to (100) and (110) surfaces makes SS even less pronounced at the (111) surface[5]. Induction of surface localized electronic structures by deposition of few foreign atoms to form superstructures was mostly on semiconductor surfaces[11–14], but less frequently on metals surfaces, e.g. Pb/Cu(100)-c(4×4)[15], Bi/Au(110)-1×4[16], and Pb/Au(111)-(5.77×5.77) R21.5[17]. Such a method has been rarely applied to Pb(111) because of its interactive nature to form alloy surfaces with foreign atoms[18–23]. In this paper, we deposited Au atoms onto Pb(111) surface specifically at a low temperature of 40 K and consequently a

[1]Department of Physics, National Tsing Hua University, Hsinchu 30013, Taiwan. [2]National Synchrotron Radiation Research Center (NSRRC), Hsinchu 30076, Taiwan. [3]Institute of Physics, Academia Sinica, Taipei 11529, Taiwan. [4]Physics Division, National Center for Theoretical Sciences, Taipei 10617, Taiwan. [5]These authors contributed equally: Wei-Chuan Chen and Chin-Hsuan Chen. ✉email: jeng@phys.nthu.edu.tw; sjtang@phys.nthu.edu.tw

superstructure phase of Au/Pb(111)-3×3 formed. Moreover, three new SS bands were observed to exist within and around the Pb bulk projected band gap centered at the surface zone boundary $\overline{M}_{Pb(111)}$. Their characteristics as well as their contributions towards the interesting properties at the surfaces are discussed.

Results and discussion

Figure 1a shows the calculated energy band structures of a 24-layer Pb(111) slab. The purple color indicates the weight of the surface component. As reported previously[5], there is a non-inverted $6sp$ bulk band gap ranging from − 8.3 to − 3.7 eV projected to the surface zone center $\overline{\Gamma}$. With the top band edge p-type and bottom band edge s-type, the SS is unlikely to exist within the band gap according to Shockley's model[9]. Our focus is rather at the surface zone boundary $\overline{M}$, where a projected bulk band gap ranges between − 2.14 eV at the bottom bulk band edge (BBBE) and 0.42 eV at the top bulk band edge (TBBE). This gap originates from the strong SOC of $6p$ bands[5]; the main orbital components of TBBE and BBBE are both p-type, which doesn't fit Shockley's model, either[9]. Figure 1b shows the measured energy band dispersions of Pb(111) at RT in the symmetry direction $\overline{\Gamma M}_{Pb(111)}(\overline{M}_{Pb(111)}$ at 1.03 Å^{-1}). This band gap spans in k space as a rhombus centered at $\overline{M}_{Pb(111)}$ due to the mirror-image symmetry with respect to it. The calculated subbands in Fig. 1a are superimposed onto the measured one as shown in Fig. 1c. Note that the calculation is based on a slab model so the calculated subbands are mainly discrete QWS bands. However, both the bulk band edges of the rhombus gap centered at $\overline{M}_{Pb(111)}$ as well as the measured Pb bulk band dispersing from the energy just below Fermi level at $\overline{\Gamma}$ down to about − 4 eV at $\overline{M}_{Pb(111)}$ are well reproduced. In their calculation for Pb(111) electronic structures, Wurde et al.[5] predicted that there two surface resonance (SR) states near TBBE and BBBE at $\overline{M}_{Pb(111)}$ [S_1 and S_2 of Fig. 3 in Ref. 5]. However, no measured counterparts have been ever observed.

We cooled down the Pb(111) substrate to 40 K and then deposited few Au atoms onto it. Figure 2a,b exhibit LEED patterns of Pb(111) before and after Au deposition at an electron energy of 40 eV. The red circles enclose the Pb(111)-1×1 spots and other spots emerging between them after Au deposition are 3×3 spots. Note that the 2/3 order spots of 3×3 are coincident with $\sqrt{3} \times \sqrt{3}$R30° spots; however, the intensities of 1/3 and 2/3 order spots, as seen in Fig. 2b, are about even, making the possibility of the existence of $\sqrt{3} \times \sqrt{3}$R30° phase unlikely. Figure 2c also shows the LEED pattern after Au deposition at 70 eV, where the Pb(111)-1×1 spots are brighter than those in Fig. 2b due to the change in diffraction conditions. The measured energy band structures of Pb(111) and Au/Pb(111)-3×3 are displayed in Fig. 2d,e, respectively for comparison. As observed, the rhombus bulk band gap centered at $\overline{M}_{Pb(111)}$ is occupied by two SS bands, S_1 and S_2. A third band, S_3, disperses beneath the BBBE of the rhombus bulk band gap. Photon-energy dependent measurement, as shown in the Fig. S1 of supplementary material, confirms their 2-dimensional (2D) nature. The faint trace of the measured intense Pb bulk band in Fig. 2d can be still detected, as indicated by an arrow, in the measured spectrum of Au/Pb(111)-3×3 in Fig. 2e. When the superstructure Au/Pb(111)-3×3 forms, the 3×3 lattice can inflict an extra reciprocal vector $\vec{G}_{3\times3}$ to the momentum of photoelectrons. This means that the final-state band is altered and the observed bulk band observed in Pb(111) due to the direct transition can diminish[24]. The energy distribution curves (EDCs) of
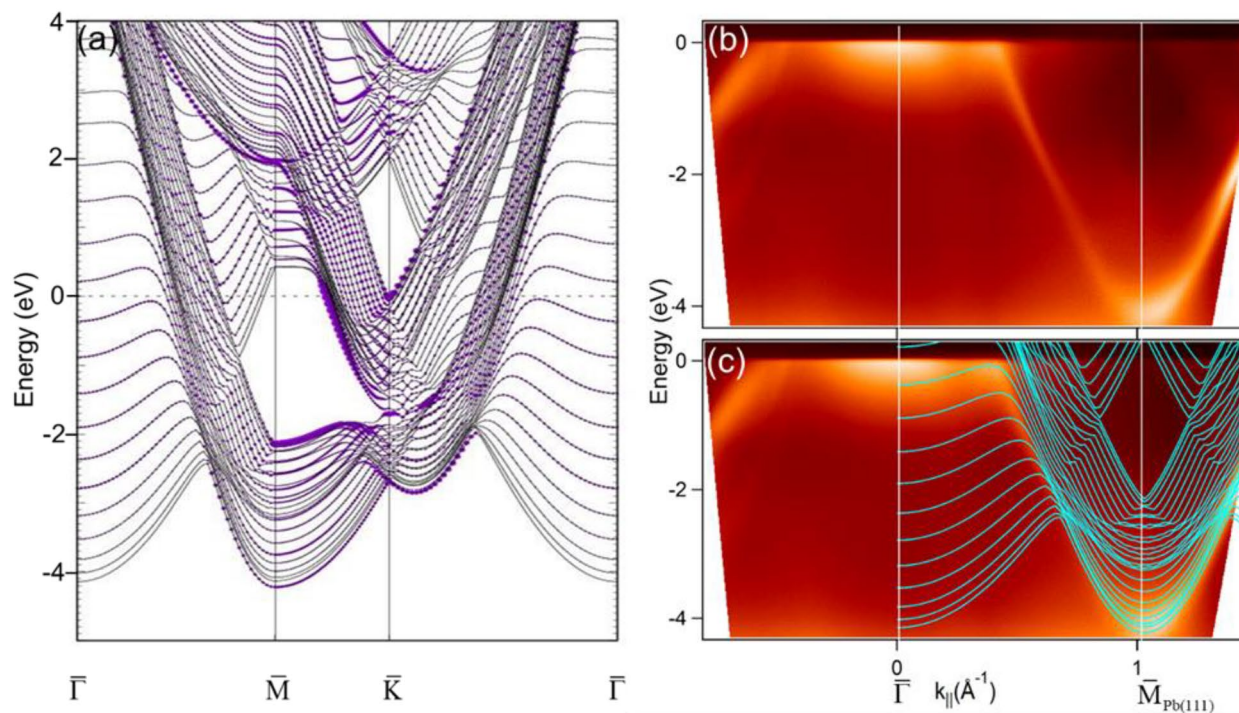

Figure 1. (**a**) The calculated energy band structures of a 24-layer Pb(111) slab. The purple color indicates the weight of the surface component. (**b**) The measured energy band structure along the symmetry direction $\overline{\Gamma M}_{Pb(111)}$ at RT. (**c**) Overlap of the calculated bands in (**a**) with the measured ones in (**b**).
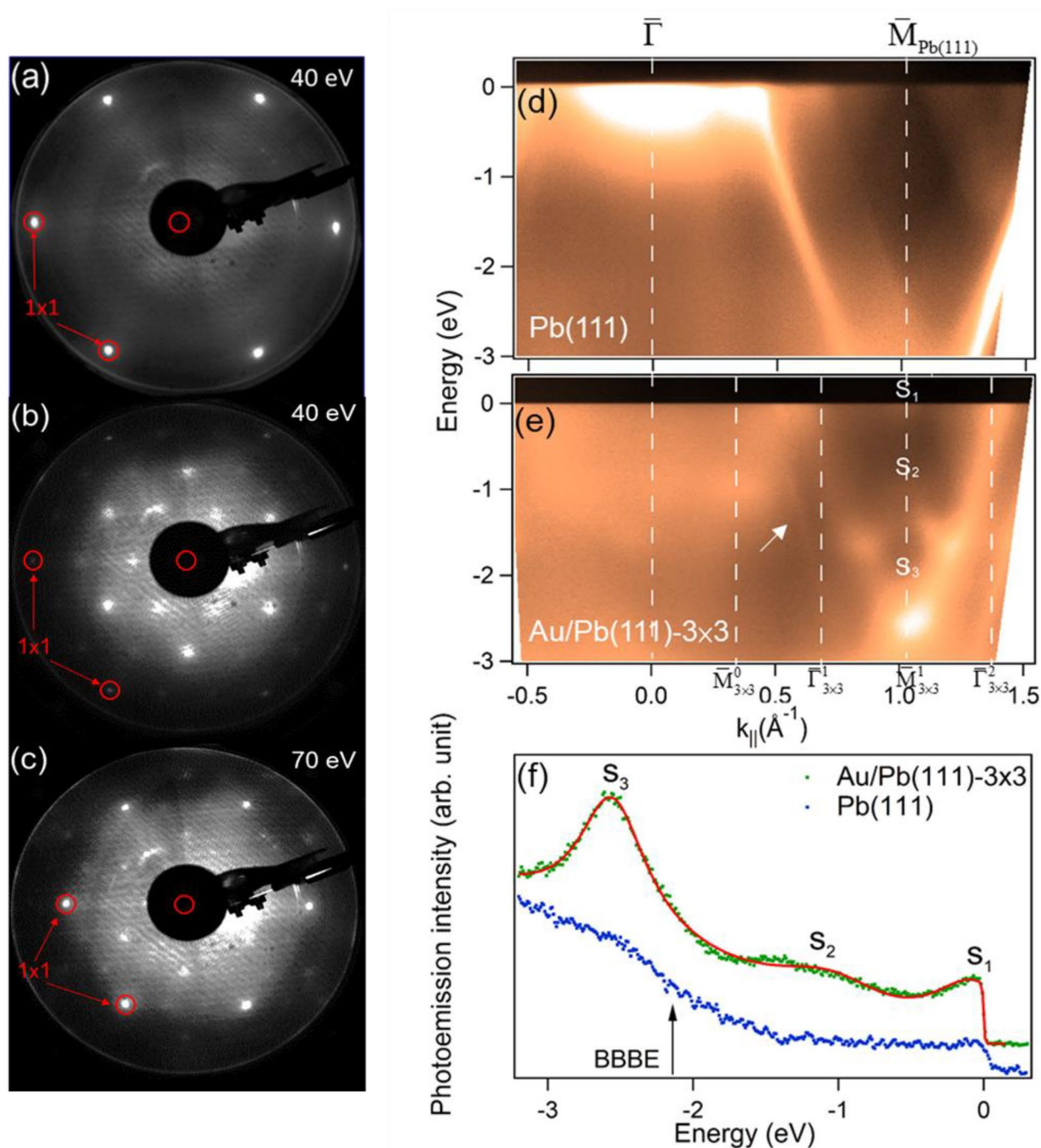
Figure 2. (**a**) LEED pattern of a clean Pb(111) surface. (**b**) and (**c**) LEED patterns of Pb(111) adsorbed with dilute Au atoms at electron energies of 40 eV and 70 eV. (**d**) The measured energy band structures of Pb(111) along the symmetry direction $\overline{\Gamma}\overline{M}_{Pb(111)}$. (**e**) The measured energy band structures of Au/Pb(111)-3×3 along the symmetry direction $\overline{\Gamma}\overline{M}_{Pb(111)}(\overline{\Gamma}^0_{3\times3} - \overline{M}^0_{3\times3} - \overline{\Gamma}^1_{3\times3} - \overline{M}^1_{3\times3} - \overline{\Gamma}^2_{3\times3})$. (**f**) The extracted EDCs at $\overline{M}_{Pb(111)}$ of clean Pb(111) (blue) and Au/Pb(111)-3×3 (green). The red curve is the fitting to the EDC of the Au/Pb(111)-3×3.

Pb(111) and Au/Pb(111)-3×3 at $\overline{M}_{Pb(111)}$ ($\overline{M}^1_{3x3}$) are extracted and shown in Fig. 2f. The peaks for S_1, S_2, and S_3 are at the energy positions of −0.02, −1.05, and −2.56 eV based on a fit of three Lorentzians plus a polynomial background, multiplied by a Fermi function. It is noteworthy that S_3 is closest to the energy position of BBBE so it should be related to the SR at $\overline{M}_{Pb(111)}$ in Pb(111). The arrow indicates the energy position of BBBE projected to Pb(111).

First principles calculation was implemented using a Au/Pb(111)-3×3 superstructure on a 6-ML Pb slab. In the relaxed configuration the Au atoms sit at the (fcc) hollow sites of Pb(111) as shown in the top view of the slab model in Fig. 3a. The energies for Au atoms at other positions such as top site and bridge site are higher
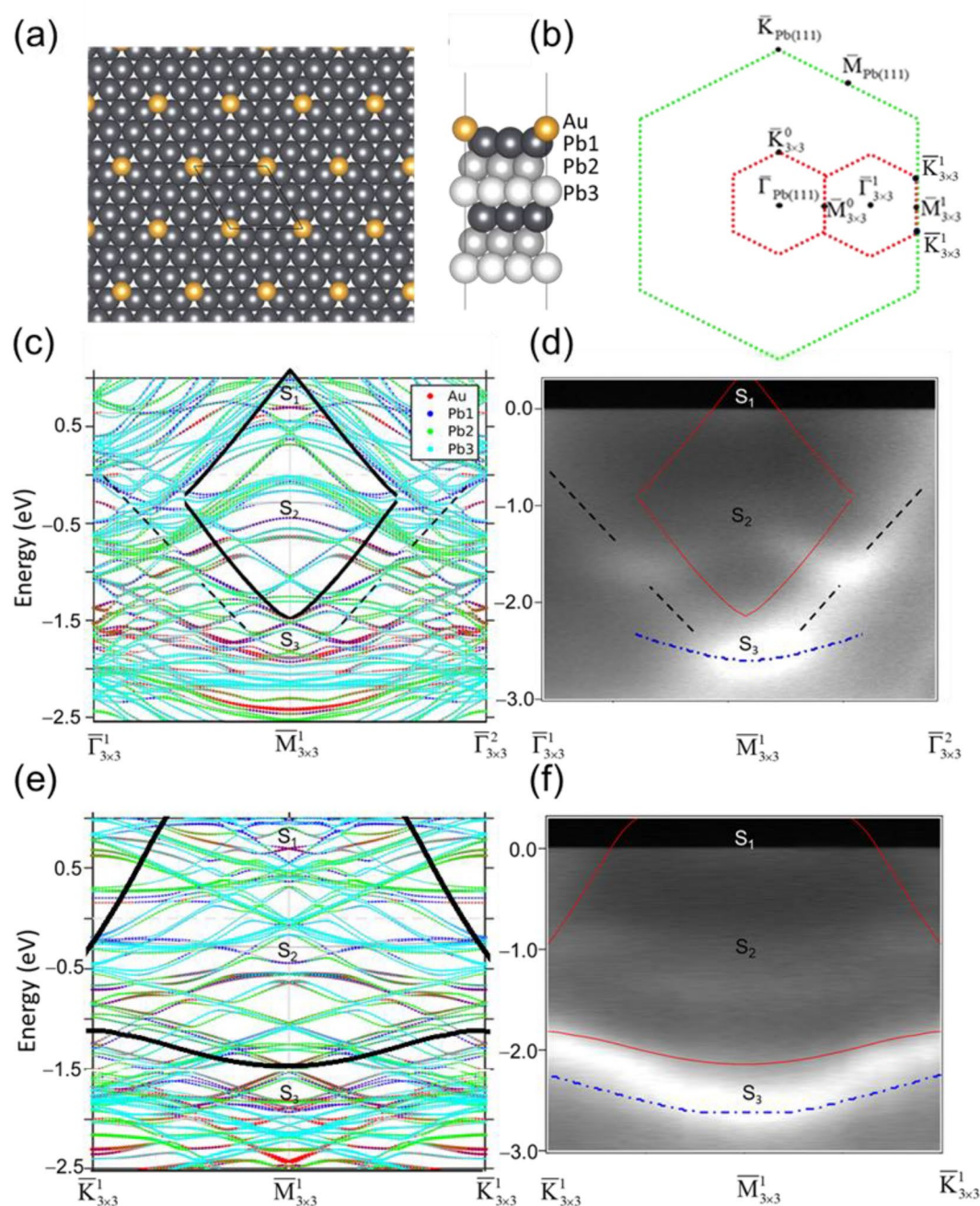
Figure 3. (**a**) The resulting Au/Pb(111)-3×3 lattice structure deduced from DFT calculation in top view and side view. (**b**) The surface brouillon zones of Pb(111) and Au/Pb(111)-3×3. (**c**) and (**d**) The calculated and measured energy band dispersions of Au/Pb(111)-3×3 in the regime $\overline{\Gamma}^1_{3\times3} - \overline{M}^1_{3\times3} - \overline{\Gamma}^2_{3\times3}$. (**e**) and (**f**) The calculated and measured energy band dispersions of Au/Pb(111)-3×3 in the regime $\overline{K}^1_{3\times3} - \overline{M}^1_{3\times3} - \overline{K}^1_{3\times3}$. The regions of Pb bulk projected band gap in both symmetry directions are enclosed by dark (red) frames in calculated (measured) bands.

than at hollow sites according to the calculation (See Fig. S2 of supplementary material). The side view shows the fcc stacking of the top Au atom and the Pb atoms beneath, among which the Pb atoms in the top three layers are labeled. The resulting calculated bands within the two symmetry regimes $\overline{\Gamma}^1_{3\times3} - \overline{M}^1_{3\times3} - \overline{\Gamma}^2_{3\times3}$ and $\overline{K}^1_{3\times3} - \overline{M}^1_{3\times3} - \overline{K}^1_{3\times3}$ around the rhombus band gap are shown in Fig. 3c, e. The surface brillouin zones of Pb(111) and Au/Pb(111)-3×3 are plotted in Fig. 3b. Figure 3d, f show the measured counterparts in the same regimes for a clear comparison. Note that an offset of 0.7 eV between the measurement and calculation is applied to achieve a reasonable match. The frames enclosing the projected bulk band gaps in both symmetry directions are superimposed. The sizes of the red, deep blue, green, and light blue circles represent the weights of the calculated bands in the top Au and the first, the second and the third Pb layer, respectively. In Figs. S3 and S4 of

4

the supplementary material, the corresponding EDCs and the further 2nd derivative image processing of the measured energy band structures in Fig. 3d, f are displayed to help clarify S_1, S_2, and S_3 bands.

As one can see, the measured S_1, S_2 and S_3 bands correspond to the calculated counterparts with dominant red and deep blue colors. S_1 band disperses across the Fermi level within the bulk band gap. S_2 band disperses through the bulk band edge to fall partially into the gap while S_3 band completely falls below BBBE and concentrates at $\overline{M}_{3\times3}^1(\overline{M}_{Pb(111)})$. In the symmetry direction $\overline{\Gamma}_{3\times3}^1 - \overline{M}_{3\times3}^1 - \overline{\Gamma}_{3\times3}^2$, there is an extra upward band outside the gap, as indicated by the dark dashed lines, connecting from S_3 to S_2 and then extending toward Fermi level. It appears that this extra band corresponds to higher aggregation density of calculated QWS subbands of the slab model. The calculation (Fig. S5 of supplementary material) shows that those subbands have more or less Au components and hence can be considered as SRs. However, their surface weights are not as large as those of S_2 and S_3 so the intensity of the extra band is substantially lower than them in Fig. 3c. In the symmetry direction $\overline{K}_{3\times3}^1 - \overline{M}_{3\times3}^1 - \overline{K}_{3\times3}^1$, such an extra band is not observed. Because the entire S_3 band dispersion is merely below the BBBE, much more extended dispersion of S_3 band is observed in this direction. Although the calculated SS bands still extend out of the rhombus Pb bulk projected band gap, only those within and just outside the gap are observed in the measurement. Calculation also shows the measured S_3 band is actually composed of aggregated SR subbands and S_2 covers two bands, the lower one of which has more surface weight in the symmetry direction $\overline{K}_{3\times3}^1 - \overline{M}_{3\times3}^1 - \overline{K}_{3\times3}^1$ so it can be identified in the measured counterpart (Fig. 3f).

Charge of the S_2 state at $M_{3\times3}^1(M_{Pb(111)})$ distributes as 43.14, 25.49, 5.88, and 9.8% in the Au and first three Pb layers (Fig. S6 of supplementary material). Its large surface weight is in line with its energy position located in the middle of bulk projected band gap[9]. The main contributing Au and Pb orbitals are Au-6s and Pb-6p_x-6p_y. S_1 state is pertinent to the conducting property of Au/Pb(111)-3×3 phase since it is near to and crosses the Fermi level. At $M_{3\times3}^1(M_{Pb(111)})$, charge is distributed at 45.0%, 17.5%, 8.75%, and 6.25% in the Au layer and the top three Pb layers (Fig. S6 of supplementary material). The main contributing Au and Pb orbitals are Au-6 s and Pb-6p_x-6p_y. Note that Wurde et al. predicted a SR band in Pb(111) at $\overline{M}_{Pb(111)}$ right at TBBE of 0.42 eV [The band labeled "S_2" of Fig. 3 of Ref. 5]. Therefore, it is likely that the S_1 state of Au/Pb(111)-3×3 is derived from this SR although its energy descends to be below TBBE. The transition temperature, T_C, of superconductivity is closely related to the DOS at the Fermi level, $N(E_f)$[3]. Therefore, the S_2 state can contribute to the surface superconductivity of Au/Pb(111)-3×3. The S_3 band, with its energy position near BBBE, is likely derived from another SR of Pb(111) [The band labeled "S_1" of Fig. 3 in Ref. 5] . The blue dashed-dot curves in Fig. 3c, d represent the calculated SR bands of Pb(111), extracted from Fig. 3 of Ref. 5 in two symmetry directions. It is evident that the SR band of Pb(111) resembles the S_3 of Au/Pb(111)-3×3 except for a slight energy offset ~ 0.06 eV. S_3 band charge at $M_{3\times3}^1(M_{Pb(111)})$ distributes as 45.38, 12.61, 5.88, and 4.2% in the Au layer and the first three Pb layers (Fig. S6 of supplementary material). The main contributing Au and Pb orbitals are Au-5d_{xz}-5d_{yz} and Pb-6p_x-6p_y. Compared to S_1 and S_2, S_3 state has quite less charge in the top three Pb layers, indicating its longer decay length into the bulk.

The similarity of S_1 and S_3 bands of Au/Pb(111)-3×3 to the two SR bands at TBBE and BBBE, respectively, centered at $\overline{M}$ of Pb(111) points out that a SR state existing at the edge of a bulk band gap in the substrate that may at first seem irrelevant can turn much more pronounced after being covered with a superstructure or thin layer made of foreign atoms. Au atoms have a higher electronegativity than Pb (2.4 vs 1.9) so Au atoms attracts electron charges of SR in Pb(111) to cause more distribution of its wave function at the interface. Intriguingly, this begs the question "Does such SR wavefunction distribution enhance the Rashba effect that requires the breaking of inversion-symmetry through the interface?" Fig. 4a,b show the spin-polarization of the calculated subbands for Au/Pb(111)-3×3 in the symmetry directions, $\overline{\Gamma}_{3\times3}^1 - \overline{M}_{3\times3}^1 - \overline{\Gamma}_{3\times3}^2$ and $\overline{K}_{3\times3}^1 - \overline{M}_{3\times3}^1 - \overline{K}_{3\times3}^1$, respectively. Green rectangles enclose S_1, S_2, and S_3 bands to guide the eye. As one can see, the Rashba splitting is negligible for S_2, and S_3 bands but relevant for S_1. The extracted Rashba constant $\alpha = \frac{2\Delta E}{k_0}$ is 1.0 eVÅ ($\Delta E = 0.016$ eV, $k_0 = 0.032$ Å^{-1}) in the symmetry direction $\overline{\Gamma}_{3\times3}^1 - \overline{M}_{3\times3}^1 - \overline{\Gamma}_{3\times3}^2$ and 3.54 eVÅ ($\Delta E = 0.0469$ eV, $k_0 = 0.0275$ Å^{-1}) in $\overline{K}_{3\times3}^1 - \overline{M}_{3\times3}^1 - \overline{K}_{3\times3}^1$. The Rashba constants α of the SS of Au(111) and the QWS of Pb(111) thin films were measured to be 0.33[25,26] and 0.044 eVÅ[8], respectively. Therefore the absorbed Au 3×3 layer on Pb(111) not only promotes the original SR state but also significantly enhance Rashba effect of it. According to the charge-distribution percentage of S_1, S_2, and S_3 over the top four layers, as described above, S_1 has more charge than S_2 at the top Au layer and the second Pb layer, hence triggering Rashba effect more effectively via considering the first Pb layer as the interface.

One remaining ambiguity for the Rashba effect is the role of Au that is also a heavy element like Pb ($Z_{Au} = 79$, $Z_{Pb} = 82$). Figure 5a,b show the spin-polarization of the calculated subbands for Cu/Pb(111)-3×3 and Ag/Pb(111)-3×3 in the symmetry direction $\overline{\Gamma}_{3\times3}^1 - \overline{M}_{3\times3}^1 - \overline{\Gamma}_{3\times3}^2$. Cu angle Ag are lighter elements ($Z_{Cu} = 29$, $Z_{Ag} = 47$). As indicated by green rectangles, one can spot the corresponding S_1 and S_2, S_3 bands with energies lower than the counterparts of Au/Pb(111)-3×3 by ~ 0.3 eV. The S_1 band is specially magnified to examine the Rashba splitting. Unlike Au/Pb(111)-3×3, the S_1 bands for Cu/Pb(111)-3×3 and Ag/Pb(111)-3×3 turn to disperse downward with splitting being small for the former and negligible for the latter. It appears that the high Z value of Au is important for the observed large Rashba splitting of the S_1 band in Au/Pb(111)-3×3. Nevertheless, it is intriguing that the S_1 band in Cu/Pb(111)-3×3 exhibits a bit more Rashba effect than Ag/Pb(111)-3×3 while Cu atom have a much lower Z value than Ag. Figure 6 shows the calculated charge distribution of S_1 state at $M_{3\times3}^1(M_{Pb(111)})$ in the Au and six Pb layers below, for the three cases. The charge distribution for Cu/Pb(111)-3×3 is clearly different, in that the charge percentages at the top Au layer and the first Pb layer are even and hence may assist Rashba effect at the interface. Above all, the actual factors involved in Rashba effect at the interface can be more. For example, pervious investigation of of Au, Cu, and Ag monolayers on W(110)[27,28] showed the SS of Au monolayer on W(110) had the least Rashba splitting. SOC contribution in opposite directions from Au and W, and the degree of overlayer-substrate hybridization were considered.
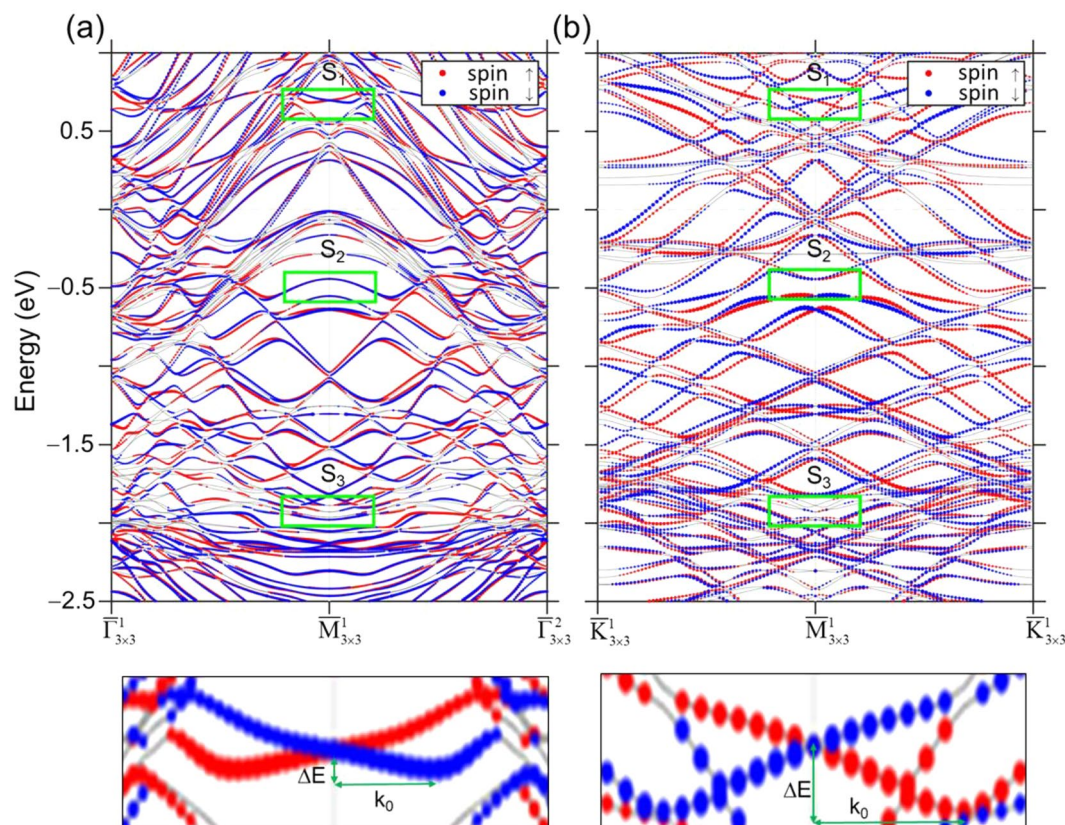
Figure 4. The calculated spin polarization of the Au/Pb(111)-3×3 energy band structures in the symmetry directions (**a**) $\overline{\Gamma}^1_{3\times3} - \overline{M}^1_{3\times3} - \overline{\Gamma}^2_{3\times3}$ and (**b**) $\overline{K}^1_{3\times3} - \overline{M}^1_{3\times3} - \overline{K}^1_{3\times3}$. Red and blue colors denote the in-plane spin polarizations in opposite directions. The insets below show the magnified views of S_1 Rashba splitting.

Conclusion

We deposited Au atoms onto Pb(111) surface at 40 K to form a Au/Pb(111)-3×3 superstructure. ARPES measurement reveals three distinct SS energy bands (S_1, S_2, and S_3) disperse within and around the rhomboidal bulk energy band gap centered at the surface zone boundary $\overline{M}^1_{3\times3}(\overline{M}_{Pb(111)})$. The calculated SS bands based on Au/Pb(111)-3×3 on a 6-layer Pb slab match the measured bands well. These three SS bands are composed of mainly Pb p orbitals and a few Au s and d orbitals. S_1 and S_3 states of Au/Pb(111)-3×3 originate from SRs at the TBBE and BBBE of Pb(111). As revealed from S_1, the Rashba effect is greatly enhanced (α = 1.0 and 3.54 eVÅ) with respect to that of Au(111) surface and the Pb(111) thin film. Calculation of Rashba splitting for corresponding S_1 bands in Cu/Pb(111)-3×3 and Ag/Pb(111) indicates the important role of Au atoms. Our results show an interesting idea that an irrelevant SR state in a substrate can be promoted by a suitable superstructure or a 2D material on the top, which can further help induce its novel property.

Experimental procedures and calculation methods

The Pb(111) single crystal substrate was cleaned by repeated cycles of sputtering with a 1.0 keV Ar$^+$ ion for an hour followed by annealing at 473 K for 30 min and the surface quality was confirmed by the observations of sharp spots in LEED. During the Au deposition for the formation of Au/Pb(111)-3×3 and the subsequent measurements, the temperature of Pb(111) was kept at 40 K using liquid He. When the temperature increases above 40 K, the PbAu alloy starts forming. A water-cooled Knudsen cell was operated at 1523 ± 10 K to deposit Au with a rate of 0.25 Å/min as calibrated from a quartz-crystal thickness monitor. ARPES measurements on Au/Pb(111)-3×3 were carried out with a Scienta R4000 energy analyzer using a p-polarized light source at 22 eV at the undulator beamline BL21B1 at the National Synchrotron Radiation Research Center (NSRRC) in Taiwan. The energy and angular resolutions were 10 meV and 0.3°.

The ab initio simulations are performed by Vienna Ab initio Simulation Package (VASP)[29,30] based on density functional theory (DFT). The exchange–correlation functional with Ceperley-Alder (CA) type local-density approximation (LDA)[31] is utilized in calculations. To simulate the surface-state electronic states, the 1 × 1 24-ML Pb(111) slab and 3 × 3 6-ML Pb(111) slab with adsorbed Au atoms on top of the Pb slab at the hollow site are considered. The size of the vacuum region used is 15 Å. The gamma-centered Monkhorst–Pack k-meshes of 24 × 24 × 1 and 12 × 12 × 1 are used, respectively. The bulk Pb lattice constant of 4.9508 Å and energy cutoff of 300 eV are adopted. The positions of adsorbed Au atoms and top two-layer of Pb are optimized until the residual atomic forces are smaller than 0.03 eV/Å. The unfolding of band structure is carried out by using the
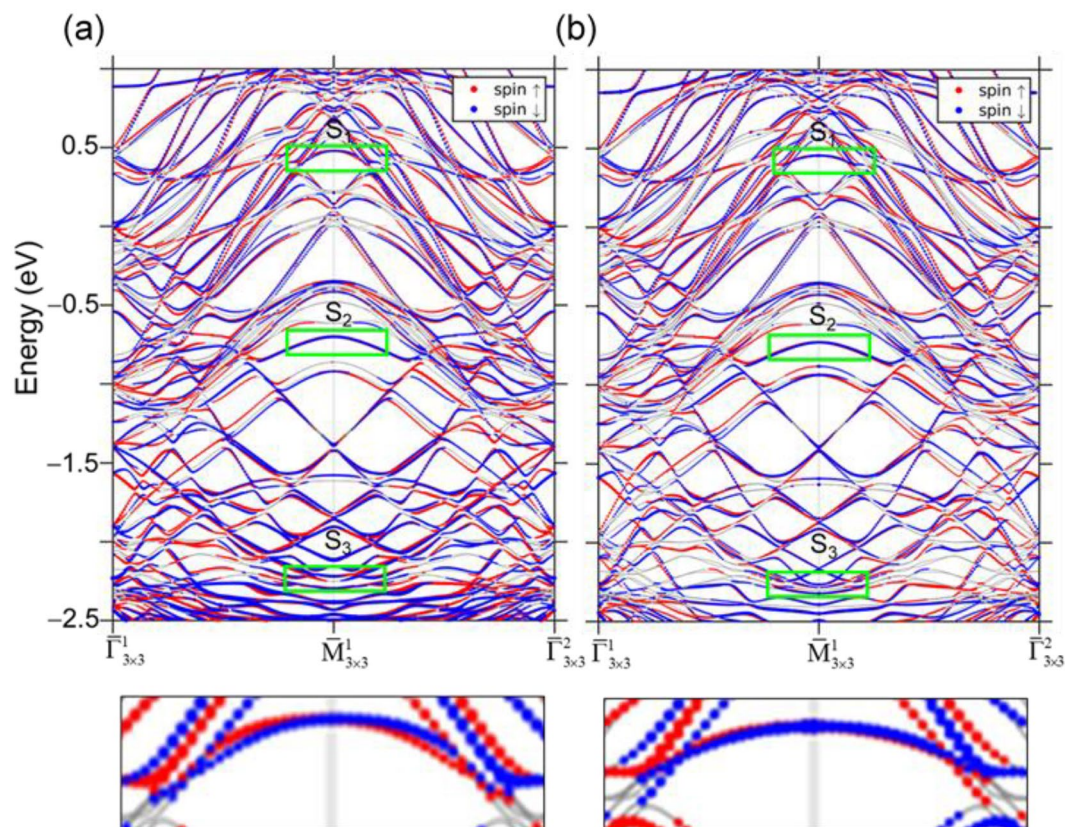
Figure 5. The calculated spin polarization of the (**a**) Cu/Pb(111)-3×3 and (**b**) Ag/Pb(111)-3×3 energy band structures in the symmetry directions $\overline{\Gamma}^1_{3\times3} - \overline{M}^1_{3\times3} - \overline{\Gamma}^2_{3\times3}$. The insets below show the magnified views of S_1 bands.
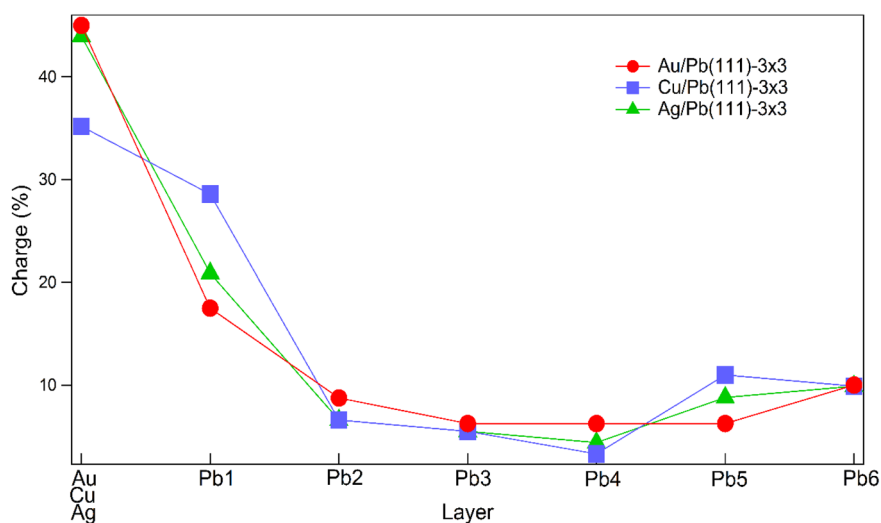

Figure 6. Calculated charge-distribution profile perpendicular to the surface for S_1 at $\overline{M}^1_{3\times3}$ ($\overline{M}_{Pb(111)}$) in Au/Pb(111)-3×3, Cu/Pb(111)-3×3 and Ag/Pb(111)-3×3.

BandUP package[32,33]. SOC is applied in the calculation. The calculation of the surface-state electronic states for Cu/Pb(111)-3×3 and Ag/Pb(111)-3×3 follows the same way.

Data availability
The datasets used and/or analyzed during the current study are available from the corresponding author on reasonable request.

References

1. Matthias, B. T., Geballe, T. H. & Compton, V. B. Superconductivity. *Rev. Mod. Phys.* **35**, 1 (1963).
2. Goy, P. & Castaing, B. High-frequency cyclotron resonance in lead and the electron–phonon interaction. *Phys. Rev. B* **7**, 4409 (1972).
3. Guo, Y. *et al.* Superconductivity modulated by quantum size effects. *Science* **306**, 1915 (2004).
4. Jia, J.-F., Li, S.-C., Zhang, Y.-F. & Xue, Q.-K. Quantum size effects induced novel properties in two-dimensional electronic systems: Pb thin films on Si(111). *J. Phys. Soc. Jpn.* **76**, 082001 (2007).
5. Wurde, K., Mazur, A. & Pollmann, J. Surface electronic structure of Pb(001), Pb(110), and Pb(111). *Phys. Rev. B* **49**, 7679 (1994).
6. Horn, K. *et al.* Electronic energy bands of lead: Angle-resolved photoemission and band-structure calculations. *Phys. Rev. B* **30**, 1711 (1984).
7. Ley, L., Kowalczyk, S. P., McFeely, F. R. & Shirley, D. A. Crystal-field effects on the apparent spin-orbit splitting of core and valence levels observed by X-ray photoemission. *Phys. Rev. B* **10**, 4881 (1974).
8. Dil, J. H. *et al.* Rashba-type spin-orbit splitting of quantum well states in ultrathin Pb films. *Phys. Rev. Lett.* **101**, 266802 (2008).
9. Davison, S. G. & Steslicka, M. *Basic Theory of Surface States* (Oxford University Press, 1992).
10. Plummer, E. W. & Gadzuk, J. W. Surface states on tungsten. *Phys. Rev. Lett.* **25**, 1493 (1970).
11. Chazalviel, J. N., Stefenel, M. & Truong, T. B. Surface states induced by metal atoms at the Si/electrolyte interface. *Surf. Sci.* **134**, 865 (1983).
12. Hasegawa, S., Tong, X., Takeda, S., Sato, N. & Nagao, T. Structures and electronic transport on silicon surfaces. *Prog. Surf. Sci.* **60**, 89 (1999).
13. Kim, J. K. *et al.* Two-dimensional electron gas formed on the indium-adsorbed Si(111)√3×√3-Au surface. *Phys. Rev. B* **80**, 075312 (2009).
14. Yaji, K. *et al.* Large Rashba spin splitting of a metallic surface-state band on a semiconductor surface. *Nat. Commun.* **1**, 17 (2010).
15. Joco, V., Martínez-Blanco, J., Segovia, P., Vobornik, I. & Michel, E. G. Surface electronic structure of Pb/Cu(100). *J. Phys. Condens. Matter* **21**, 474216 (2009).
16. Crepaldi, A. *et al.* Combined ARPES and STM study of Pb/Au(111) Moiré structure: One overlayer, two symmetries. *Phys. Rev. B* **87**, 115138 (2013).
17. Crepaldi, A. *et al.* Structural and electronic properties of the Bi/Au(110)–1 × 4 surface. *Phys. Rev. B* **88**, 195433 (2013).
18. Chen, W.-C. *et al.* Significantly enhanced giant Rashba splitting in a thin film of binary alloy. *New J. Phys.* **17**, 083015 (2015).
19. Yu, Y., Tang, Z., Jiang, Y. & Fujita, D. Surface alloying effects in the growth of Au on Pb(1 1 1) thin film. *Surf. Sci.* **602**, 3358 (2008).
20. Qi, Y. *et al.* A study of the surface structure of deposited Au on Pb film. *J. Phys. Condens. Matter* **19**, 136005 (2007).
21. Kim, J., Qin, S., Zhang, Y., Zhu, W. & Shih, C.-K. Influence of quantum well states on the formation of Au–Pb alloy in ultra-thin Pb films. *Surf. Sci.* **632**, 174 (2015).
22. Pacilé, D. *et al. Phys. Rev. B* **73**, 245429 (2006).
23. Meier, F., Dil, H., Lobo-Checa, J., Patthey, L. & Osterwalder, J. Quantitative vectorial spin analysis in angle-resolved photoemission: Bi/Ag(111) and Pb/Ag(111). *Phys. Rev. B* **77**, 165431 (2009).
24. Bocquet, F. C. *et al.* Final-state diffraction effects in angle-resolved photoemission at an organic-metal interface. *Phys. Rev. B* **84**, 241407 (2011).
25. Cercellier, H. *et al.* Interplay between structural, chemical, and spectroscopic properties of Ag/Au(111) epitaxial ultrathin films: A way to tune the Rashba coupling. *Phys. Rev. B* **73**, 195413 (2006).
26. LaShell, S., McDougall, B. A. & Jensen, E. Spin splitting of an Au(111) surface state band observed with angle resolved photoelectron spectroscopy. *Phys. Rev. Lett.* **77**, 3419 (1996).
27. Hortamani, M. & Wiesendanger, R. Role of hybridization in the Rashba splitting of noble metal monolayers on W(110). *Phys. Rev. B* **86**, 235437 (2012).
28. Shikin, A. M. *et al.* Induced Rashba splitting of electronic states in monolayers of Au, Cu on a W(110) substrate. *New. J. Phys.* **15**, 095005 (2013).
29. Kresse, G. & Furthmüller, J. Efficiency of ab-initio total energy calculations for metals and semiconductors using a plane-wave basis set. *Comput. Mater. Sci.* **6**, 15 (1996).
30. Kresse, G. & Furthmüller, J. Efficiency of ab-initio total energy calculations for metals and semiconductors using a plane-wave basis set. *Phys. Rev. B* **54**, 11169 (1996).
31. Ceperley, D. M. & Alder, B. J. Efficient iterative schemes for ab initio total-energy calculations using a plane-wave basis set. *Phys. Rev. Lett.* **45**, 566 (1980).
32. Medeiros, P. V. C., Stafström, S. & Björk, J. Effects of extrinsic and intrinsic perturbations on the electronic structure of graphene: Retaining an effective primitive cell band structure by band unfolding. *Phys. Rev. B* **89**, 041407 (2014).
33. Medeiros, P. V. C., Tsirkin, S. S., Stafström, S. & Björk, J. Unfolding spinor wave functions and expectation values of general operators: Introducing the unfolding-density operator. *Phys. Rev. B* **91**, 041116 (2015).

Acknowledgements

Author contributions

W.-C.C carried out experiments and prepared figures. C.-H.C. and A.H. carried out calculations. K.L., M.-K.D., J.-M.K., D.-S.L., and C.-M.C. assist experiments. D.M. helped with the manuscript. H.-T.J. supervised calculations. S.-J.T. led the project and wrote the manuscript.

Competing interests

The authors declare no competing interests.

Additional information

Supplementary Information The online version contains supplementary material available at https://doi.org/10.1038/s41598-023-28106-0.

Correspondence and requests for materials should be addressed to H.-T.J. or S.-J.T.

Reprints and permissions information is available at www.nature.com/reprints.

Publisher's note Springer Nature remains neutral with regard to jurisdictional claims in published maps and institutional affiliations.